Complete Open-Stopband Suppression Using Sinusoidally Modulated Anisotropic Metasurfaces

Federico Giusti, *Graduate Student Member, IEEE*, Stefano Maci, *Fellow, IEEE*, and Enrica Martini, *Senior Member, IEEE*

Abstract— A novel and general approach is presented for the complete suppression of the open-stopband (OSB) effects in circularly polarized 1-D periodic leaky-wave antennas (LWAs) using anisotropic modulated metasurfaces (MTSs). A theoretical justification of this behavior is found through the rigorous treatment of the canonical problem of an infinite homogenized impedance surface sinusoidally modulated along the propagation direction. By deriving a closed-form solution of this problem at broadside scan, it is shown that, while the sinusoidally modulated isotropic impedance exhibits a null of the attenuation constant, the complex propagation constant for the proposed anisotropic modulation has a finite value and a regular behavior. A closed-form formula for the leakage constant α is also derived, allowing for an accurate design of the aperture field amplitude. The full-wave analysis of a patch-based implementation of the MTS is in excellent agreement with the results based on the homogenized impedance model, thus demonstrating the practical applicability of the theoretical results. The elimination of the OSB behavior allows for the design of LWAs able to scan the beam from backward (BWD) to forward (FWD) without any frequency regions of blindness.

Index Terms— 1-D periodic modulation, broadside radiation, Floquet theorem, leaky-wave antennas (LWAs), metasurfaces (MTSs), open stopband (OSB), periodic structures.

I. INTRODUCTION

PLANAR antennas based on periodically modulated surface impedances have recently emerged as an effective low-profile alternative to printed arrays or reflectarrays for the realization of high gain radiators [1], [2], [3], [4], [5], [6], [7]. These antennas belong to the class of periodic leaky-wave antennas (LWAs), in which a slow wave (SW), fed by a primary source, excites a fast Floquet wave (FW), typically the $n = -1$, due to the interaction with a periodically loaded or modulated guiding structure. This radiation mechanism is well suited for frequency scanning applications, since the beam scans from backward (BWD) to forward (FWD) as the frequency increases. However, a problem of such antennas is the abrupt variation of the radiation efficiency when the beam is scanned through broadside [8]. The narrow frequency region corresponding to $n = -1$ FW radiation around broadside is usually known as the *open-stopband* (OSB) region [9]. In the
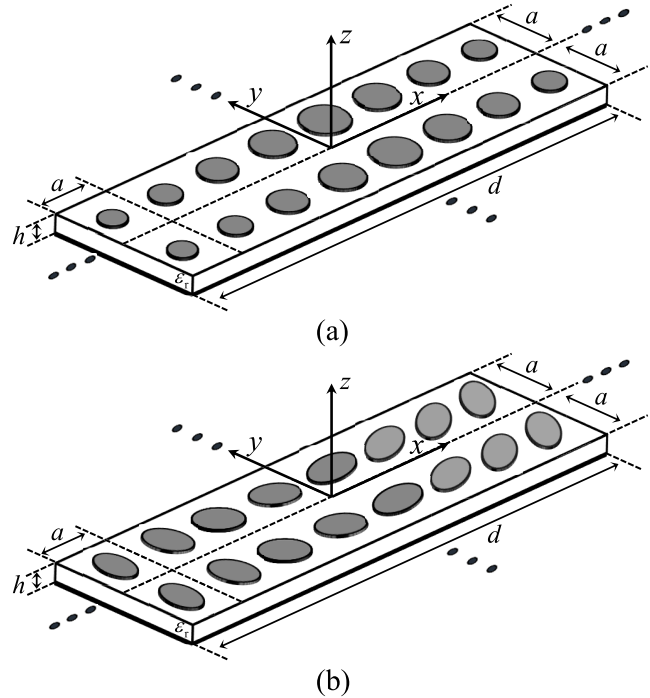
Fig. 1. (a) Schematic period of the isotropic 1-D periodically modulated patch-type LWA. (b) Schematic period of the anisotropic 1-D periodically modulated patch-type LWA. The three black dots aligned with the x-/y-direction both in (a) and (b) define the 2-D periodicity of the two antennas in the respective directions.

OSB, the leakage constant typically varies rapidly assuming first a highly peaked value and then dropping to zero. This is due to the contradirectional coupling between a pair of FWs, resulting in a standing-wave effect and in a consequent mismatch [8]. For a finite structure, this implies an increase in the reflection coefficient and a drop in the realized gain. Several techniques were proposed in the last years for solving or mitigating the OSB problem.

A noteworthy approach to mitigate the OSB problem is based on small-perturbation theory and consists of introducing in each modulation period a pair of identical quarter wave-length spaced scatterers, so that the waves reflected by the two scatterers almost cancel each other [10], [11]. However, in the general case, the practical design requires some ad hoc optimization. A systematic design approach based on mutual scattering cancellation through the introduction of quarter-wave transformers or matching stubs was proposed

in [12] and experimentally validated in [13]. In [14], [15], [16], [17], and [18], more general studies on the suppression of the OSB were conducted, exploiting transverse, longitudinal, or double asymmetry in the structure to satisfy frequency-balancing and Q-balancing conditions. This can be seen as a generalization of the approach for OSB suppression in composite right-/left-handed (CRLH) LWAs [19], [20]. More recently, the transversal asymmetry design principle was applied in [21] using two similar but *unequal* discontinuities inside the unit cell, and this approach was then generalized in [22]. Moreover, several realizations of LWAs with improved broadside radiation have been published, including an SIW LWA with periodic longitudinal slots [23], a single-layer spoof-plasmon-mode LWA [24], and an asymmetrically modulated Goubau line [25].

In this work, we demonstrate a novel approach to design circularly polarized LWAs with completely suppressed OSB using 1-D periodically modulated *anisotropic* metasurfaces (MTSs) with a proper sinusoidal profile of the homogenized impedance boundary conditions (IBCs). Although this kind of modulation has been already employed to design centrally fed broadside pointing-modulated MTS antennas [6], [26], the OSB issue has not been investigated yet. A preliminary study has been conducted in [27] and [28]. A complete analysis including full-wave verification is done in this article for the first time. Starting from the rigorous analysis of the canonical problem of an infinite periodic structure with sinusoidally homogenized IBC, the OSB suppression is theoretically demonstrated through the derivation of a closed-form solution for the leakage constant and of the relative complex coefficients of the FWs at broadside. These results and the smooth behavior around broadside are then numerically substantiated by solving the dispersion equation in a wider frequency range. Furthermore, the practical applicability of the concept is verified by implementing the anisotropic impedance profile through elliptical patches [29] (see Fig. 1) and performing a full-wave analysis of the resulting structure. Full-wave results are in excellent agreement with the ones found for the homogenized structure, thus confirming the complete suppression of the OSB. Finally, numerical results relevant to a finite length structure are presented to better assess the impact of the OSB suppression in practical MTS LWAs.

Unlike approaches that rely on the introduction of reflection canceling elements, the strategy proposed here offers a remarkable solution to the OSB problem in both propagation directions of the SW. This results in broadside radiation with opposite circular polarizations, enabling dual-polarized operation. In addition, this strategy eliminates the need for ad hoc optimization for specific geometries, as it only requires the synthesis of elements implementing a certain impedance profile, which is a well-established and systematic process. It is important to note that the sinusoidal shape of the modulation should not be seen as a restriction or limitation. On the contrary, it can be effectively implemented using artificial surfaces with arbitrary constitutive unit cells. Moreover, the general expression of the modulation contains a sufficient number of degrees of freedom (namely, average reactance and modulation index) to allow for independent control over the
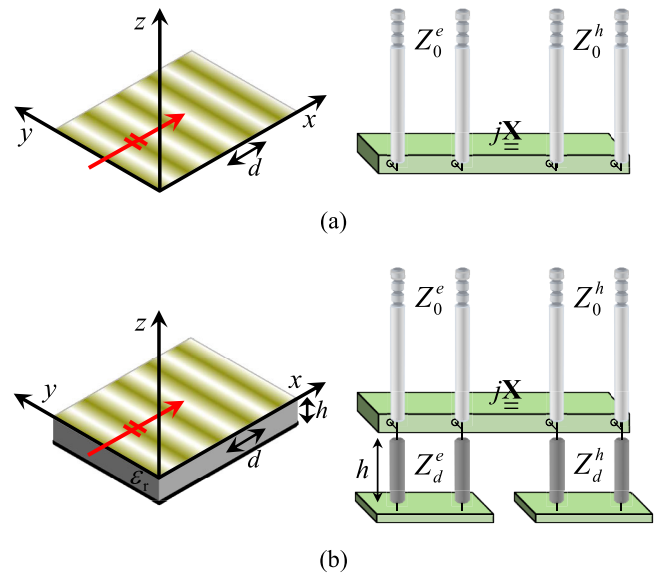

Fig. 2. Geometry for the problem of the 1-D sinusoidally modulated impedance on the left and relevant equivalent transmission line model on the right for (a) IIBC and (b) PIBC on a grounded slab.

broadside pointing frequency and the value of the attenuation constant.

This article is organized as follows. Section II defines the canonical problem for the homogenized, infinite periodic structure, and the relevant dispersion equation. Section III derives the closed-form solution at broadside. The analytical solution is compared in Section IV with the one obtained by numerically solving the dispersion equation. Radiation from a finite structure is considered in Section V. Throughout this article, besides the proposed anisotropic periodic structure, an isotropic one, exhibiting the OSB behavior, is also considered for the sake of comparison. Finally, the conclusions are drawn in Section VI.

II. PROBLEM FORMULATION FOR DISPERSION ANALYSIS

In this section, we derive the equations describing the propagation and radiation characteristics of waves supported by a sinusoidally modulated anisotropic reactance surface. The analysis approach employed here is a generalization of the one proposed in [30] for a scalar sinusoidally modulated impenetrable impedance. This generalization was originally introduced in [31, Sec. III]. A similar approach, applicable to an arbitrary periodic modulation profile, was developed in [32] by incorporating the Fourier series expansion of the impedance. The impedance surface sits in the xy plane of a Cartesian coordinate system, and it is invariant along the y-direction and modulated along the x-direction, which coincides with the propagation direction of the wave. The structure is assumed to be lossless. Throughout this article, an $\exp(j\omega t)$ time dependence is assumed and suppressed.

Two types of reactive IBCs will be considered in this article. The first one is an *impenetrable* IBC (IIBC), described by a tensor, which relates the tangential components of the total

electric and magnetic fields on the surface as follows:

$$\mathbf{E}_t(z=0^+) = j\underline{\underline{\mathbf{X}}} \cdot \hat{z} \times \mathbf{H}_t(z=0^+). \quad (1)$$

On the other hand, the *penetrable* IBC (PIBC) relates the tangential component of the electric field to the discontinuity of the tangential magnetic field according to this relationship

$$\mathbf{E}_t(z=0) = j\underline{\underline{\mathbf{X}}} \cdot \hat{z} \times \left[\mathbf{H}_t(z=0^+) - \mathbf{H}_t(z=0^-)\right]. \quad (2)$$

The geometry for the problem treated with the two afore-mentioned IBCs (IIBC and PIBC), together with their corresponding equivalent transmission line models, is shown in Fig. 2. Two different equivalent transmission lines are associated with the transverse magnetic (TM, or e) and transverse electric (TE, or h) components. For PCB-based MTSs, the reactance tensor in the IIBC accounts for both the metallic cladding and the grounded slab, as illustrated in Fig. 2(a). However, the IIBC can also be applied to other several kinds of MTS implementations, including the ones based on bed of nails and corrugations [33]. The PIBC is used here as a homogenized model of the metallic cladding of MTSs realized in PCB technology, assuming that this condition holds on top of a grounded dielectric slab of thickness h and relative permittivity ϵ_r. In this case, the grounded dielectric slab is accounted for by a section of short circuited transmission line, as shown in Fig. 2(b), while the metallic cladding is represented by a shunt load that, in the most general case, couples the TE and TM transmission lines. As widely demonstrated in the literature [34], this is the most accurate model for this kind of structures, since it allows to rigorously account for the space and frequency dispersion of the grounded slab.

Both the conditions in (1) and (2) can be expressed through the following compact unified representation:

$$\mathbf{E}_t(z=0) = j\underline{\underline{\mathbf{X}}} \cdot \mathbf{J} \quad (3)$$

where $\mathbf{J}$ assumes the meaning of equivalent current ideally flowing either on top of the surface for the IIBC case or in the metallic cladding for the PIBC case. In both cases, $\underline{\underline{\mathbf{X}}}$ is the reactance tensor, which is written in a matrix form as follows:

$$\underline{\underline{\mathbf{X}}} = \begin{bmatrix} X_{xx} & X_{xy} \\ X_{yx} & X_{yy} \end{bmatrix} = \begin{bmatrix} X_{ee} & X_{eh} \\ X_{he} & X_{hh} \end{bmatrix} \quad (4)$$

where the second equality denotes the fact that, for Cartesian components and propagation along the x-direction, the xx and yy components correspond to the ee and hh components, respectively. The extra diagonal entries in (4) account for the coupling between different polarizations.

All the entries of the reactance tensor are assumed uniform along the y-direction and periodically modulated with period d along the x-direction. Due to the periodic nature of the problem, currents and fields can be represented in terms of FWs (space harmonics), respectively, as follows:

$$J_x(x) = J^e(x) = \frac{1}{d} \sum_{n=-\infty}^{\infty} I_n^e e^{-jk_{x,n}x} \quad (5)$$

$$J_y(x) = J^h(x) = \frac{1}{d} \sum_{n=-\infty}^{\infty} I_n^h e^{-jk_{x,n}x} \quad (6)$$

$$E_x(x) = E^e(x) = \frac{1}{d} \sum_{n=-\infty}^{\infty} G_{EJ}^e(k_{x,n}) I_n^e e^{-jk_{x,n}x} \quad (7)$$

$$E_y(x) = E^h(x) = \frac{1}{d} \sum_{n=-\infty}^{\infty} G_{EJ}^h(k_{x,n}) I_n^h e^{-jk_{x,n}x} \quad (8)$$

where $k_{x,n} = k_{x,0} + 2\pi n/d$ are the Floquet transverse wavenumbers and $G_{EJ}^{e,h}$ are the TM and TE spectral Green's functions of the problem. These latter in the IIBC case are given by

$$G_{EJ}^{e,h}(k_{x,n}) = -Z_0^{e,h}(k_{x,n}) \quad (9)$$

where $Z_0^e = \eta_0 k_{z,n}/k_0$, $Z_0^h = \eta_0 k_0/k_{z,n}$, $k_{z,n} = -j\sqrt{k_{x,n}^2 - k_0^2}$, and η_0 and k_0 are the free-space impedance and wavenumber.

In the PIBC case, we have instead

$$G_{EJ}^{e,h}(k_{x,n}) = -Z_0^{e,h}(k_{x,n}) \parallel Z_{gs}^{e,h}(k_{z,n}) \quad (10)$$

where $Z_{gs}^{e,h} = jZ_d^{e,h}\tan(k_{zd,n}h)$ is the grounded slab contribution, with $Z_d^e = \eta_d k_{zd,n}/k_d$, $Z_d^h = \eta_d k_d/k_{zd,n}$, $k_{zd} = \sqrt{k_d^2 - k_{x,n}^2}$, and $\eta_d = \eta_0/\sqrt{\epsilon_r}$ and $k_d = \sqrt{\epsilon_r}k_0$ are the dielectric impedance and wavenumber, respectively.

The TM and TE components of the vector modal voltage $\mathbf{V}_n$ of the nth FW are defined as follows:

$$V_n^e = \int_{-d/2}^{d/2} E^e(x)e^{jk_{x,n}x}dx = G_{EJ}^e(k_{x,n})I_n^e \quad (11)$$

$$V_n^h = \int_{-d/2}^{d/2} E^h(x)e^{jk_{x,n}x}dx = G_{EJ}^h(k_{x,n})I_n^h. \quad (12)$$

The dominant (zero-indexed) FW is an SW with propagation constant close to the one corresponding to the average impedance. When, for some index n, the real part of the transverse propagation constant falls in the visible range (i.e., $|\mathfrak{Re}\{k_{x,n}\}| < k_0$), the mode is an LW, and the transverse wavenumbers of all the FWs acquire an imaginary part, accounting for radiation. In the following, we will use β and α to denote the real and imaginary parts of the propagation constant of the dominant mode, i.e., $k_{x,0} = \beta - j\alpha$. For the analysis of the OSB problem, we are interested in the case $\beta d = 2\pi$, corresponding to broadside radiation of the $n = -1$ FW ($\mathfrak{Re}\{k_{x,-1}\} = 0$). Notice that in this case, we have $\mathfrak{Re}\{k_{x,0}\} = -\mathfrak{Re}\{k_{x,-2}\}$, i.e., the $n = 0$ and $n = -2$ FWs are two SWs traveling in opposite directions with the same phase velocity.

We consider now two different cases: a sinusoidally modulated *isotropic* impedance and a sinusoidally modulated *anisotropic* impedance.

A. Isotropic (Scalar) Impedance

We assume in this case that the extra-diagonal entries of the reactance tensor are identically zero; this implies a complete decoupling between the TE and TM components of the fields, and the vector problem can be reduced to a scalar one.

We consider the following sinusoidal behavior for the diagonal entries of the reactance tensor:

$$X_{pp}(x) = \overline{X}_{pp}\left[1 + M\cos\left(\frac{2\pi}{d}x\right)\right] \quad (13)$$

where M is the modulation index, $\overline{X}_{pp}$ represents the average reactance, and $p = e, h$. An inductive (capacitive) impenetrable $\overline{X}_{ee}$ ($\overline{X}_{hh}$) will support a TM (TE) modal solution with no

cutoff frequency. The propagation and radiation characteristics of the supported modes can be found with the rigorous procedure presented in [30] and briefly summarized in the following.

Substituting (3), together with (5) and (6), into (11) and (12), we obtain the following infinite set of linear homogeneus equations in which, due to the sinusoidal nature of the modulation, each equation involves only three modes:

$$M I_{n-1}^{e,h} + D_n^{e,h} I_n^{e,h} + M I_{n+1}^{e,h} = 0, \quad n = 0, \pm 1, \pm 2, \dots \quad (14)$$

with

$$D_n^{e,h} = 2 \left(1 + j \frac{G_{EJ}^{e,h}(k_{x,n})}{\overline{X}} \right). \quad (15)$$

This infinite set of equations possesses a nontrivial solution if the infinite determinant of the set vanishes. As shown in [30] for the IIBC case, this condition can be written in terms of rapidly convergent continued fractions and efficiently solved numerically with respect to the variable $k_{x,0}$. The solution provides the complex wavenumber of the fundamental $n = 0$ FW, from which all the other harmonics wavenumbers are immediately obtained by considering the displacement factor $2\pi n/d$. The same approach can be also applied in the PIBC case [34]. This procedure, therefore, allows for the accurate derivation of the complete field distribution and the propagation characteristics of the supported modes.

B. Anisotropic (Tensorial) Impedance

In this section, we consider the case of a full reactance tensor with the following behavior of its entries:

$$X_{ee}(x) = \overline{X} \left[1 + M \cos \left(\frac{2\pi}{d} x \right) \right]$$

$$X_{eh}(x) = X_{he}(x) = \overline{X} M \sin \left(\frac{2\pi}{d} x \right)$$

$$X_{hh}(x) = \overline{X} \left[1 - M \cos \left(\frac{2\pi}{d} x \right) \right] \quad (16)$$

where, similar to the isotropic case, M is the modulation index and $\overline{X}$ represents the average reactance. Notice that this anisotropic impedance modulation is the same used in [6] and [26] to design broadside pointing, circularly polarized, modulated MTS antennas.

The problem is solved by generalizing to the vector case the procedure introduced in Section II-A as shown in [34]. Substituting (3), together with (5) and (6), into (11) and (12), we obtain the following transverse resonance equations:

$$\underline{\underline{M}}^- \mathbf{I}_{n-1} + \underline{\underline{D}}_n \mathbf{I}_n + \underline{\underline{M}}^+ \mathbf{I}_{n+1} = 0, \quad n = 0, \pm 1, \pm 2, \dots \quad (17)$$

where $\mathbf{I}_n = [I_n^e \ I_n^h]^T$,

$$\underline{\underline{D}}_n = \begin{bmatrix} D_n^e & 0 \\ 0 & D_n^h \end{bmatrix} \quad (18)$$

and

$$\underline{\underline{M}}^+ = (\underline{\underline{M}}^-)^* = M \begin{bmatrix} 1 & j \\ j & -1 \end{bmatrix}. \quad (19)$$

Equation (17) can be viewed as a double infinite set of linear homogeneous equations with an infinite number of vector unknowns $\mathbf{I}_n$, which can be solved with an approach analogous to the one outlined for the isotropic case.

III. CLOSED-FORM SOLUTION AT BROADSIDE

In this section, we derive a closed-form solution for (14) and (17) when $\beta d = 2\pi$, corresponding to the broadside pointing of the $n = -1$ FW.

A. Isotropic Impedance

At broadside scan, it has been proved in [8] that

$$k_{z,n}^2 = k_{z,-(n+2)}^{*2}, \quad n = 0, \pm 1, \pm 2, \dots \quad (20)$$

Since, for the principal branch, all $k_{z,n}$, $n \neq -1$, are located on the respective proper Riemann sheet with $\Im\{k_{z,n}\} < 0$, one has from (20) that

$$D_n^{e,h} = \left(D_{-(n+2)}^{e,h} \right)^*, \quad n \neq -1. \quad (21)$$

Using (14) to express the ratios $I_{-2}^{e,h}/I_{-1}^{e,h}$ and $I_0^{e,h}/I_{-1}^{e,h}$ as infinite continued fractions involving D_n for $n < -1$ and $n > -1$ only, respectively [30], in view of (21), it is possible to show that $(I_{-2}^{e,h}/I_{-1}^{e,h}) = (I_0^{e,h}/I_{-1}^{e,h})^*$. After plugging the two expressions into the equation for $n = -1$, and noticing that $D_{-1}^{e,h}$ is complex, it is possible to conclude that $I_{-1}^{e,h} = 0$; that is, at broadside, the $n = -1$ FW amplitude vanishes, and hence, $\alpha = 0$. Furthermore, we have $I_0^{e,h} = -I_{-2}^{e,h}$, giving rise to a standing wave in the invisible region, which stores reactive energy and creates the OSB. This behavior is numerically substantiated in Section IV-A.

B. Anisotropic Impedance

In order to solve the system of equations in (17) when $\beta d = 2\pi$, let us define the auxiliary variables

$$I_n^+ = I_n^e + j I_n^h \quad (22)$$

$$I_n^- = I_n^e - j I_n^h \quad (23)$$

that allow us to rewrite

$$I_n^e = \frac{I_n^+ + I_n^-}{2} \quad (24)$$

$$I_n^h = \frac{I_n^+ - I_n^-}{j2}. \quad (25)$$

It is noted that the current coefficients I_{-1}^+ and I_{-1}^- are associated with the two opposite circular polarizations.

Substituting (22) and (23) into (17), we can obtain, for a generic index n, the two following linear homogeneous equations:

$$M I_{n-1}^+ + D_n^e \left(\frac{I_n^+ + I_n^-}{2} \right) + M I_{n+1}^- = 0 \quad (26)$$

$$M I_{n-1}^+ - D_n^h \left(\frac{I_n^+ - I_n^-}{2} \right) - M I_{n+1}^- = 0 \quad (27)$$

or equivalently

$$4M I_{n-1}^+ + \left(D_n^e - D_n^h \right) I_n^+ + \left(D_n^e + D_n^h \right) I_n^- = 0 \quad (28)$$

$$\left(D_n^e + D_n^h \right) I_n^+ + \left(D_n^e - D_n^h \right) I_n^- + 4M I_{n+1}^- = 0. \quad (29)$$

At the broadside condition, we have $D_{-1}^e \simeq D_{-1}^h = D_{-1}$. Then, after combining (28) for $n = 0$ and (29) for $n = -1$, we can obtain the following relationships:

$$\frac{I_{-1}^+}{I_0^+} = \frac{2 \left(D_0^e - D_0^h \right)}{\left[D_{-1} \left(D_0^e + D_0^h \right) - 8M \right]} \quad (30)$$
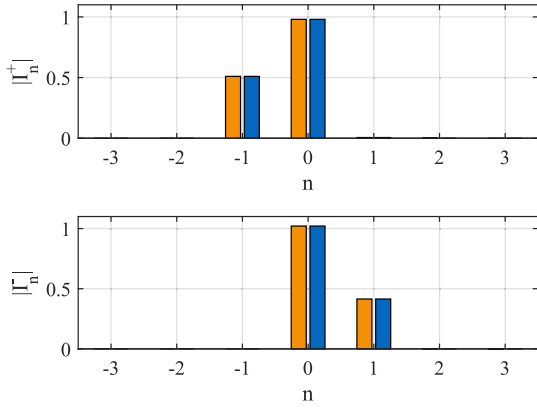
Fig. 3. Magnitude of the FW coefficients I_n^+ and I_n^- at the broadside frequency obtained with the analytical (orange bars) and numerical (blue bars) solutions.

Fig. 4. Magnitude of the FWD and BWD FW coefficients I_n^+ and I_n^- at the broadside frequency obtained with the analytical solution in (32)–(35).

$$\frac{I_0^-}{I_0^+} = \frac{D_{-1}(D_0^e - D_0^h)}{8M - [D_{-1}(D_0^e + D_0^h)]}. \tag{31}$$

We now consider the set of linear homogeneous equations consisting of (28) and (29) for $n < 1$ plus (28) for $n = -1$, and we notice that its determinant is different from zero. This last result allows us to conclude that

$$I_n^+ = 0, \quad n = -2, -3, \ldots \tag{32}$$
$$I_n^- = 0, \quad n = -1, -2, \ldots \tag{33}$$

We notice that the condition $I_{-1}^- = 0$ implies that at broadside scan, the $n = -1$ FW is perfectly circularly polarized. For the solution with $\beta d = -2\pi$, one finds $I_{-1}^+ = 0$, corresponding to the opposite circular polarization.

A closed-form solution can be obtained for any harmonic by successively solving for $n = 0, 1, 2, \ldots$ first (29) for the index n and then (28) for $n + 1$. Finally, the solution is iteratively expressed as follows:

$$I_{n+1}^+ = -\frac{D_n^e + D_n^h}{4M}I_n^+ - \frac{D_n^e - D_n^h}{4M}I_n^- \tag{34}$$
$$I_{n+1}^- = -\frac{D_n^e + D_n^h}{4M}I_n^+ - \frac{D_n^e - D_n^h}{4M}I_n^- \tag{35}$$

respectively, from (28) for index $n + 1$ and (29) for index n.

The derived formulas for the FW relative amplitudes have been validated against the numerical solution of (17). These latter are obtained by truncating the infinite linear system at $|n| = 10$ and analyzing the eigenvector relevant to the zero-valued eigenvalue of the system matrix in order to derive the relative amplitudes of the current modes. A perfect agreement has been found between analytical and numerical solutions, thus validating the derivation. An example is shown in Fig. 3. It is relevant to the case of a PIBC over a dielectric slab with thickness $h = 0.508$ mm and relative permittivity $\epsilon_r = 9.8$, with modulation period $d = 9$ mm, average reactance -484 Ω, and modulation index 0.36. These parameters have been selected to have the $n = -1$ FW radiating broadside at 29 GHz. The result obtained at this frequency clearly shows that, as opposed to what happens for the case of sinusoidally modulated isotropic impedance, in this case, the coefficient of the $n = -1$ FW does not vanish at the broadside condition, and the $n = -2$ FW is not excited ($I_{-2}^+ = I_{-2}^- = 0$).
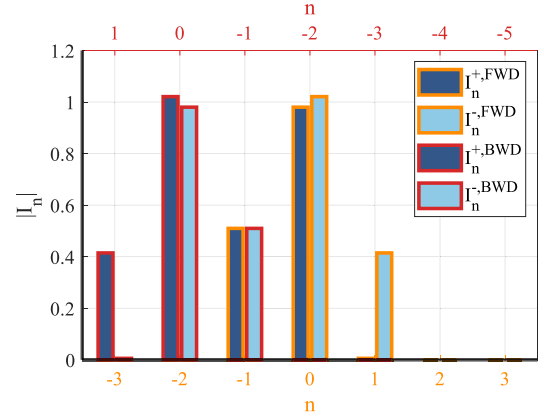
For a deeper understanding of the origin of the OSB suppression, Fig. 4 provides additional insight into the mode decoupling mechanism. It displays the magnitudes of the I_n^+ and I_n^- FW coefficients of the expansions associated with SWs propagating along the positive x-direction (FWD) and along the negative x-direction (BWD) at the broadside frequency, as obtained with the analytical solution given by (32)–(35). The amplitudes of the FWD and BWD FWs are depicted as bars with orange and red edges, respectively, and their numbering is shown in the corresponding colors at the bottom and top of the figure. The two scales have been properly displaced to align degenerate modes of the two expansions. I_n^+ and I_n^- are represented in blue and light-blue colors, respectively. It is evident that $\forall n \neq -1$, when the magnitude of an FWD FW is nonzero, the magnitude of the degenerate BWD FW is zero and vice versa (although the figure displays only a limited number of FWs, this is rigorously true for all of them). In the case $n = -1$, both the FWD and BWD FWs are equally excited. However, since the two modes are oppositely circularly polarized, they do not couple. Consequently, the complete absence of contradirectional coupling between degenerate FWs is responsible for the OSB suppression. It should be noted that such decoupling cannot be achieved in the isotropic case, since the $n = -1$ harmonic exhibits the same linear polarization for the two contradirectional waves.

This analysis also clearly shows that a similar OSB suppression effect is also obtained on the same modulated MTS when the SW traveling in the opposite direction is excited, with broadside radiation in the opposite circular polarization. Hence, the proposed anisotropic MTS LW concept possesses a remarkable peculiarity: not only it effectively eliminates the OSB problem bidirectionally, but it also can generate either right-handed or left-handed circular polarization simply by switching the excitation position from one endpoint to the other. This feature sets it apart from all the solutions for OSB suppression which are focused on linear polarization and only work for a single propagation direction of the SW. Furthermore, the proposed design procedure is not based on a specific geometry-driven design. Instead, it presents a generally implementable approach that can be applied to any type of MTS unit cell geometry, as long as an homogenized description holds. In particular, since the OSB suppression has been demonstrated for both penetrable and impenetrable

homogenized anisotropic BCs, the concept can be applied to various types of MTS implementations. Finally, it is noted that the proposed solution does not refer to a single specific modulation profile, but rather to a "family" of modulations characterized by two degrees of freedom (namely, the average reactance and the modulation index), which permit an independent control of the broadside pointing frequency and of the attenuation constant. The sinusoidal profiles are the ones providing the most compact Fourier series and, therefore, allowing for a relatively simple closed-form solution for the FW coefficients. It is possible that a similar effect could be also obtained for other types of anisotropic impedance modulations [32]; however, such extension is not explored in this article for the sake of simplicity.

The knowledge of the FW coefficients allows us to also obtain a closed-form expression of the leakage constant α by equating the power radiated by the $n = -1$ FW to the power lost by the slow FWs.

Let us denote with $P_{SW}(x)$ the time average active power (per unit length along the y-direction) carried along the x-direction by the SWs. We know that it decays with attenuation constant α, i.e.,

$$P_{SW}(x) = P_{SW}(0)e^{-2\alpha x}. \tag{36}$$

Since the system is passive and lossless, the rate of variation of $P_{SW}(x)$ must balance out the one of the power radiated by the LW

$$\frac{dP_{SW}(x)}{dx} = -\frac{dP_{LW}(x)}{dx} = -S_{LW} \tag{37}$$

where S_{LW} represents the active power density per unit surface radiated by the LW, associated with the $n = -1$ FW only, that can be expressed as follows:

$$S_{LW} = \frac{1}{2}\Re\left\{\mathbf{I}_{-1}^* \underline{\underline{\mathbf{G}}}(k_{x,-1})\mathbf{I}_{-1}\right\} \tag{38}$$

where $\underline{\underline{\mathbf{G}}}(k_{x,-1}) = \text{diag}[G_{EJ}^e(k_{x,-1}), G_{EJ}^h(k_{x,-1})]$. Therefore, from (36)–(38) and considering that, at the broadside condition, $|I_{-1}^e| = |I_{-1}^h|$ and $G_{EJ}^e(k_{x,-1}) = G_{EJ}^h(k_{x,-1})$, the following closed-form solution for the leakage constant can be derived:

$$\alpha = \frac{\left|\frac{I_{-1}^e}{I_0^e}\right|^2 \Re\left\{G_{EJ}^e(k_{x,-1})\right\}}{\frac{P_{SW}(0)}{|I_0^e|^2}}. \tag{39}$$

The ratio I_{-1}^e/I_0^e is obtained from (24) and (25) along with (30) and (31), and $P_{SW}(0)/|I_0^e|^2$ can be calculated by integrating the real part of the x component of the Poynting vector along the z-direction. As an illustrative example, we report here the explicit expression for the case of a PIBC over a grounded slab of thickness h and relative permittivity ϵ_r, where the dominant mode is TM [31]. In this case, we have

$$P_{SW}(0) = \frac{\omega\epsilon_0 |I_0^e|^2}{4} \sum_{n \neq -1} \frac{k_{x,n}\left|G_{EJ}^e(k_{x,n})\right|^2 \left|\frac{I_n^e}{I_0^e}\right|^2}{\sin^2(k_{zd,n}h)}$$
$$\times \left[\frac{\epsilon_r}{k_{zd,n}^2}\left(h + \frac{\sin(2k_{zd,n}h)}{2k_{zd,n}}\right) + \frac{\sin^2(k_{zd,n}h)}{\alpha_{z,n}^3}\right] \tag{40}$$

with $\alpha_{z,n} = \sqrt{k_{x,n}^2 - k_0^2}$. In (40), all the TM slow FWs are taken into account; however, since the majority of the power is carried by the dominant (zero-indexed) FW, we can include only its contribution. Furthermore, we can approximate (40) at the first order for small values of $k_{zd,0}h$ as follows:

$$P_{SW}(0) = \frac{\omega\epsilon_0 k_{x,0}|G_{EJ}^e(k_{x,0})|^2\left|I_0^e\right|^2}{4}\left[\frac{2\epsilon_r}{hk_{zd,0}^4} + \frac{1}{\alpha_{z,0}^3}\right]. \tag{41}$$

The accuracy of (39) with (40) is tested in Section IV-A through a comparison with numerical results, showing an excellent agreement. The availability of a closed-form expression of the leakage constant as a function of the modulation parameters allows for a very precise control of the radiating field amplitude tapering.

IV. NUMERICAL RESULTS IN THE BROADSIDE REGION

In this section, we numerically analyze the dispersion behavior of the infinite periodically modulated impedance surfaces introduced in Section II in a frequency range around the broadside frequency. The average impedance is assumed to be inductive and capacitive for the IIBC and PIBC cases, respectively, since these are the model suitable to describe patch-type MTS with a backing ground plane, the most common implementation for MTS antennas in the microwave range [1], [2], [6].

Accordingly, a ω and $1/\omega$ dependence is assumed for the average reactance $(\overline{X})$ in the IIBC and PIBC cases, respectively, with ω being the angular frequency. With this frequency dependency, the homogenized impedance models are numerically solved, starting from (14) and (17) derived in Section II-A and II-B, respectively, in order to verify the existence/absence of the OSB. For the PIBC case, the frequency behavior of the FW coefficients is also analyzed, and the accuracy of the homogenized model is verified against full-wave simulations of a practical MTS implementation based on elliptical patches. Those simulations have been carried out using the spectral MoM described in [34] with the basis functions proposed in [29]. More details on the methods employed for dispersion analysis can be found in [34]. The synthesis of the elliptical patches has been carried out using a local periodicity assumption. In this context, the use of the PIBC model, by rigorously accounting for the spatial dispersion of the grounded slab, allows for an improved agreement with the homogenized model with respect to the approaches based on IIBC [1], [5].

A. Isotropic PIBC Model

The numerical results shown in this section are relevant to the case of a dielectric slab with thickness $h = 0.508$ mm and relative permittivity $\epsilon_r = 9.8$, modulation period $d = 9$ mm, average reactance -429 Ω, and modulation index 0.36 (qualitatively similar results have been obtained for different slabs and modulation parameters). These parameters have been selected to have the $n = -1$ FW pointing broadside at 29 GHz.

The case of *isotropic* homogenized PIBC is considered first. For this case, the equivalent tensor in (4) is diagonal ($X_{eh}(x) = X_{he}(x) = 0$), and the supported modes are purely TM. The complex propagation constant of the dominant mode is numerically derived by solving the non linear determinantal equation
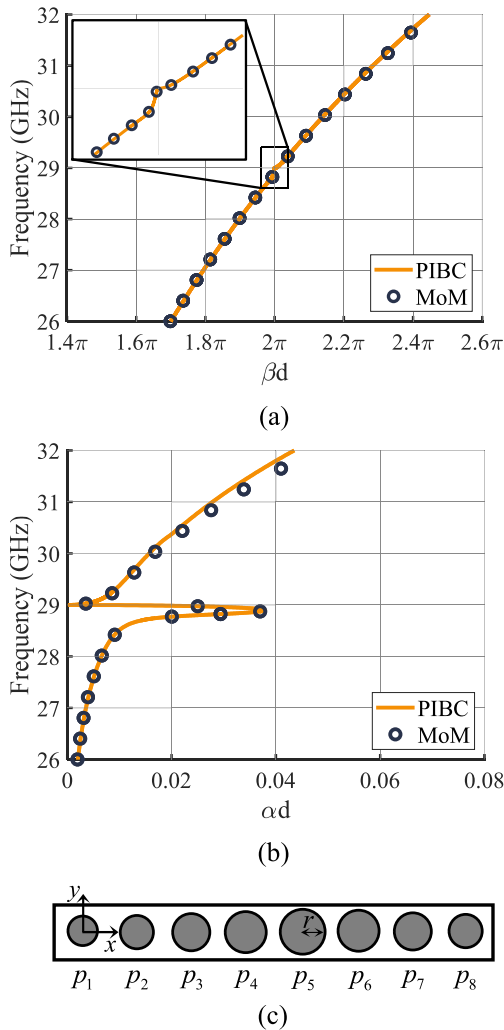
(a)

(b)

(c)

Fig. 5. Dispersion analysis of the 1-D sinusoidally modulated isotropic MTS: comparison between the homogenized PIBC model and the spectral periodic MoM described in [29]. (a) Normalized propagation constant (βd) of the fundamental, $n = 0$, FW. (b) Normalized leakage constant (αd). (c) Top view of the modulation period for the patch-type structure analyzed with the MoM with r being the patch radius.

TABLE I
RADII OF THE CIRCULAR PATCHES FOR THE 1-D SINUSOIDALLY MODULATED ISOTROPIC MTS ILLUSTRATED IN FIG. 5(c)

patch$_\#$	p_1	p_2	p_3	p_4	p_5	p_6	p_7	p_8
r (mm)	0.34	0.35	0.38	0.41	0.43	0.41	0.38	0.35

relevant to the truncated version of the infinite linear system in (14). The resulting propagation and leakage constants are represented by the continuous line in Fig. 5(a) and (b), respectively. As can be seen, exactly at the broadside frequency of 29 GHz (i.e., the frequency at which the dispersion curve in Fig. 5(a) crosses $\beta d/\pi = 2$) the leakage constant approaches a null point, as predicted by the theoretical analysis. The perturbation due to the OSB has also a small effect on the propagation constant, as can be appreciated in the zoomed-in view in Fig. 5(a).

In order to assess the accuracy of this homogenized model in the prediction of the performances of real structures, the continuous isotropic PIBC profile has been discretized con-
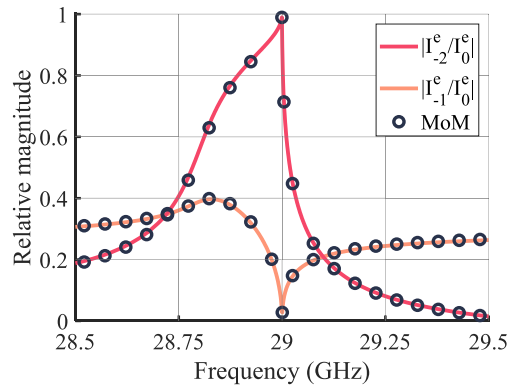

Fig. 6. Frequency variation of the relative magnitude of the $n = -1$ and $n = -2$ complex FWs with respect to the fundamental harmonic, $n = 0$, in the 1-D isotropic periodically modulated MTS computed using the homogenized PIBC model (continuous lines) and the spectral MoM in [34] (blue markers).

sidering eight unit cells of size $a = 1.25$ mm per period and implemented through circular patches [see Fig. 5(c)], whose radii are reported in Table I. This synthesis step is based on maps generated invoking the local microperiodicity approximation [34]. The resulting structure has been analyzed through the rigorous spectral MoM described in [34], and the relevant results are shown by the blue markers in Fig. 5(a) and (b). As can be seen, an excellent agreement is found with the results relevant to the homogenized problem, which confirms the existence of an OSB issue in practical isotropic-modulated MTSs.

For a better comprehension of this phenomenon, the frequency behavior of the FW current coefficients has also been calculated from the eigenvector of both the homogenized problem and its patch-based implementation. The magnitude of the ratios I_{-2}^e/I_0^e and I_{-1}^e/I_0^e is shown in Fig. 6, showing also in this case an excellent agreement between the two models. As predicted by the theoretical analysis, the magnitude of the $n = -1$ FW drops to zero ($I_{-1}^e = 0$) when $\beta d/\pi = 2$, corresponding to broadside radiation. In the same frequency range, the relative magnitude of the $n = -2$ FW exhibits a peak, and $I_{-2}/I_0 = -1$ at $\beta d/\pi = 2$.

B. Anisotropic PIBC Model

In this section, we consider the case of an anisotropic PIBC modulated according to the law in (16). The stack up and modulation parameters are the same as in Section IV-A, except for the average reactance, which is now set to $-484\ \Omega$ to obtain broadside radiation at 29 GHz.

The propagation and leakage constants derived from the numerical solution of the homogenized problem are represented by the continuous lines in Fig. 7(a) and (b), respectively. These results confirm the complete suppression of the OSB effect, since both the two constants have a smooth monotonic behavior in the whole considered frequency band, showing no indication of a stopband behavior. The value of the leakage constant obtained using the closed-form expression in (39) is also shown by an asterisk in Fig. 7(b), showing an excellent accuracy.

Also in this case, the continuous anisotropic PIBC profile has been then discretized considering eight unit cells of size $a = 1.25$ mm per period and implemented through elliptical
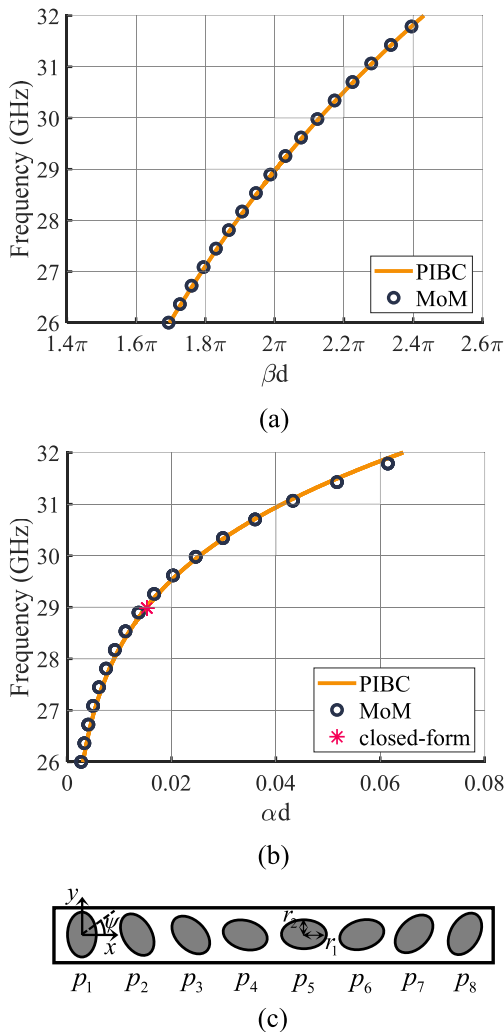
(a)

(b)

(c)

Fig. 7. Dispersion analysis of the 1-D sinusoidally modulated anisotropic MTS: comparison between the homogenized PIBC model and the spectral MoM described in [29]. (a) Normalized propagation constant (βd) of the fundamental, $n = 0$, FW. (b) Normalized leakage constant (αd); the asterisk represents the result of the closed-form expression in (39). (c) Top view of the modulation period for the elliptical patch-based implementation of the MTS with r_1 and r_2 being the semimajor and semiminor axes, respectively, and ψ the rotation angle of the major axis with respect to the x-axis.

TABLE II

GEOMETRICAL PARAMETERS FOR THE ELLIPTICAL PATCHES OF THE 1-D
SINUSOIDALLY MODULATED ISOTROPIC MTS ILLUSTRATED IN FIG. 7(c)

patch#	p_1	p_2	p_3	p_4	p_5	p_6	p_7	p_8
r_1 (mm)	0.45	0.45	0.46	0.45	0.45	0.45	0.46	0.45
r_2 (mm)	0.3	0.29	0.29	0.3	0.3	0.3	0.29	0.29
ψ (deg.)	90	113	135	156	0	24	45	67

patches [see Fig. 7(c)], whose parameters are reported in Table II. A spectral MoM with the basis functions proposed in [29] has been used to derive the propagation constant of the supported mode. The results are shown by the blue markers in Fig. 7(a) and (b) and are in excellent agreement with the analysis based on the PIBC model. The slight difference between the two models at the higher frequencies can be attributed to the simplified assumption made to describe the frequency behavior of the equivalent reactance in the homogenized model.
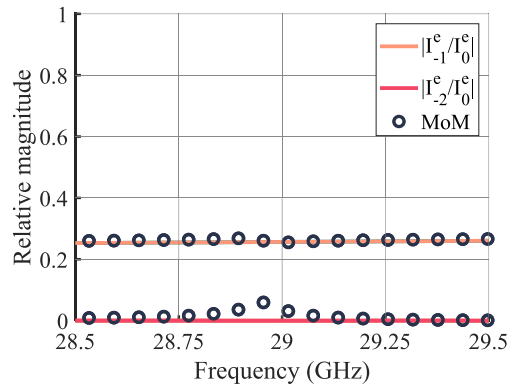

Fig. 8. Frequency variation of the relative magnitude of the $n = -1$ and $n = -2$ TM complex FW components with respect to the TM component of the fundamental harmonic, $n = 0$, in the 1-D anisotropic periodically modulated MTS computed using the homogenized PIBC model and the ad hoc spectral MoM described in [34].

As for the isotropic case, the relative complex amplitude of the FWs coefficients is also computed in a frequency band around the broadside frequency (29 GHz), and the results for $|I^e_{-1}|/|I^e_0|$ and $|I^e_{-2}|/|I^e_0|$ are shown in Fig. 8. As can be seen, the amplitude of the $n = -1$ FW does not exhibit any drop and has a smooth, flat behavior in all the considered frequency band for both the homogenized and the full-wave models. Although not reported here, the same behavior has been verified for the corresponding TE component. On the other hand, the $|I^e_{-2}|$ coefficient is practically zero in the whole frequency band according to the homogenized model. The small increase at the broadside frequency predicted by the MoM analysis (reaching $0.03|I^e_0|$ at 29 GHz) can be attributed to the discretization of the continuous anisotropic IBC profile, and it is sufficiently small not to affect the antenna behavior. Even though not shown here, both the TM and TE amplitudes of the $n = -2, -3, \ldots$, FWs are practically zero, in accordance with the derivation in Section II. Although not reported here, it has been verified through full-wave analysis that introducing small dielectric losses does not affect the complete suppression of the OSB.

C. Isotropic Versus Anisotropic IIBC Models

For the sake of completeness, this section reports the numerical results of dispersion analysis for the case of IIBC, leading to conclusions similar to the ones drawn for the PIBC case. The first case analyzed is relevant to a sinusoidally modulated *isotropic* IIBC characterized by an average reactance of 210 Ω and a modulation index of 0.36. These parameters have been selected to have the $n = -1$ FW pointing broadside at 29 GHz. The numerically derived propagation and leakage constants of the fundamental FW are represented by the blue line in Fig. 9. The OSB effect can be appreciated by the vanishing of the attenuation constant in Fig. 9(b) and by the perturbation of the propagation constant visible in the zoomed-in view in Fig. 9(a). In the same figure, the green dashed lines represent the results relevant to an *anisotropic* IIBC sinusoidally modulated in accordance with (16) with an average reactance of 215 Ω and a modulation index of 0.25. As is apparent, in this case, the curves are extremely regular, indicating the absence of the OSB.
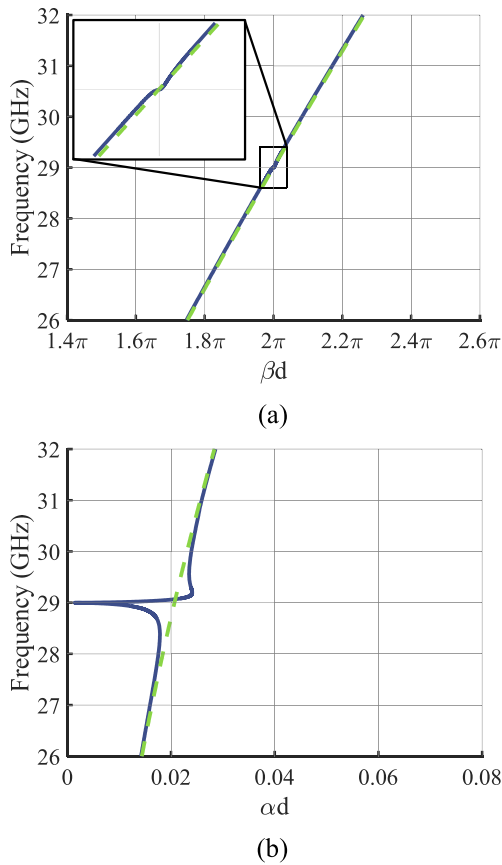
(a)

(b)

Fig. 9. Dispersion analysis of 1-D isotropic and anisotropic sinusoidally modulated IIBC surfaces. (a) Normalized propagation constant (βd) of the fundamental, $n = 0$, FW. (b) Normalized leakage constant (αd).

V. NUMERICAL RESULTS FOR A FINITE STRUCTURE

In this section, the effect of the OSB suppression on practical finite structures is investigated. Two LWAs based on the isotropic and anisotropic patch-type MTSs introduced in Sections IV-A and IV-B, respectively, have been simulated using the commercial finite-element solver ANSYS HFSS. Both the analyzed structures consist of 20 modulation periods.

For each structure, a single line of patches disposed along the x-direction has been simulated, with periodic boundary conditions along the y-direction (transverse to propagation) and radiation boundary on top. Two wave ports are set at the extremes of each antenna along the x-direction, and transitions to the average impedances are designed using circular patches in order to match the bare grounded slab to the desired average impedance.

The simulated reflection coefficients are represented in Fig. 10(a). As can be seen, due to the presence of strong reflections in the OSB, the simulated reflection coefficient of the isotropic structure increases up to -4 dB around the broadside frequency of 29 GHz. On the other hand, the simulated reflection coefficient for the anisotropic case is very low in all the considered frequency range, with a value lower than -27 dB at 29 GHz. Fig. 10(b) shows the simulated copolar realized gains at 29 GHz in the xz cut plane as a function of the observation angle θ. For the isotropic antenna, the presence of the OSB causes a drop of the realized gain of around 3.7 dB compared with the anisotropic one. On the other hand, the
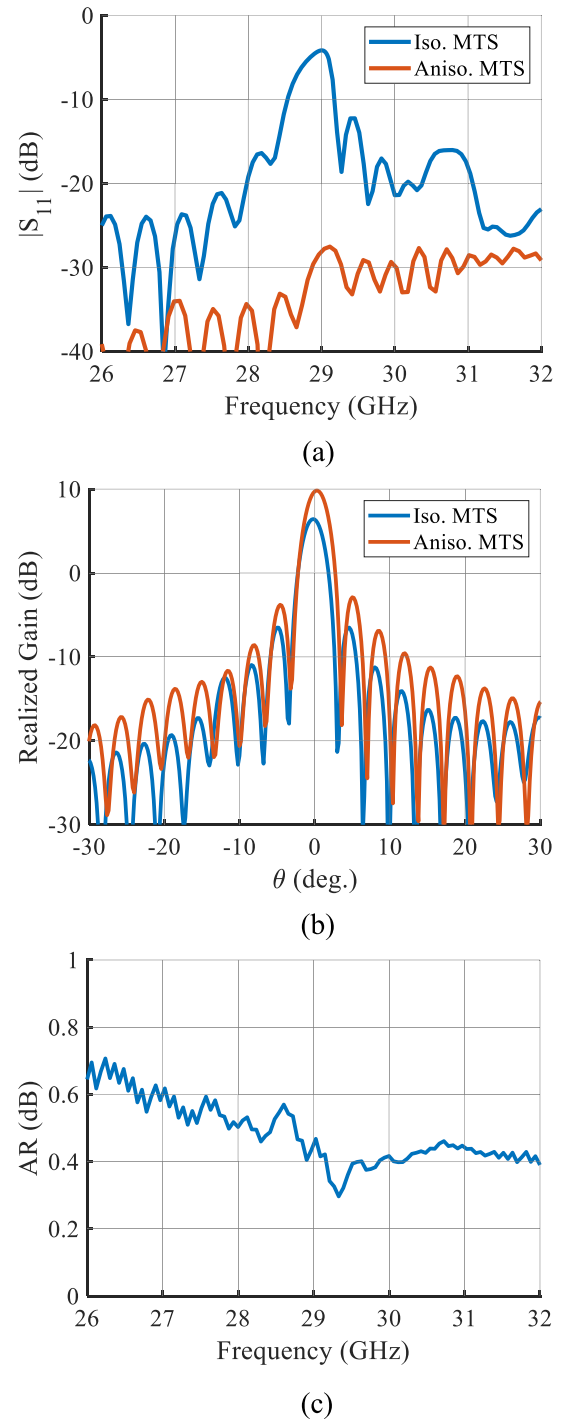

(a)

(b)

(c)

Fig. 10. Full-wave simulation of 20-macroperiod long strips for the isotropic and anisotropic sinusoidally modulated patch-type MTSs whose macroperiods is illustrated in Figs. 5(c) and 7(c), respectively. The geometrical parameters of the patches are reported in Tables I and II, respectively. (a) Reflection coefficient as a function of frequency. (b) Realized gain at 29 GHz as a function of the observation angle θ. (c) AR of the anisotropic MTS as a function of frequency.

realized gain of the anisotropic antenna increases smoothly with frequency across the considered band (not shown here), with no discernable dip at the broadside direction. Notice that the polarization of the radiated field is linear in the isotropic case and circular in the anisotropic one. The axial ratio (AR)

of this latter is reported in Fig. 10(c), showing a value smaller than 1 dB in the whole bandwidth.

VI. Conclusion

We have presented a design rule to completely suppress the OSB behavior in 1-D-modulated MTSs, based on a closed-form anisotropic impedance profile. The general validity of the approach has been demonstrated by deriving an analytic solution for the complex FWs coefficients and the leakage constant at broadside scan. The derived formulas have also been successfully validated against numerical calculations. Furthermore, the absence of the OSB effect has also been numerically verified through the full-wave analysis of a patch-type MTS implementing the proposed impedance profile, thus demonstrating the practical applicability and robustness of the approach. Finally, the impact of the OSB suppression on practical finite radiating structures based on modulated MTSs has been illustrated.

The proposed approach naturally provides a perfectly circularly polarized radiation at broadside, with the possibility to obtain opposite circular polarizations by feeding the aperture from opposite sides. The extension to the case of linear polarization can be done through component cancellation either by feeding the same aperture simultaneously from the two sides or by using a combination of subapertures producing opposite circular polarizations. This aspect will be addressed in future research.

References

[1] B. H. Fong, J. S. Colburn, J. J. Ottusch, J. L. Visher, and D. F. Sievenpiper, "Scalar and tensor holographic artificial impedance surfaces," *IEEE Trans. Antennas Propag.*, vol. 58, no. 10, pp. 3212–3221, Oct. 2010.

[2] A. M. Patel and A. Grbic, "A printed leaky-wave antenna based on a sinusoidally-modulated reactance surface," *IEEE Trans. Antennas Propag.*, vol. 59, no. 6, pp. 2087–2096, Jun. 2011.

[3] G. Minatti, S. Maci, P. De Vita, A. Freni, and M. Sabbadini, "A circularly-polarized isoflux antenna based on anisotropic metasurface," *IEEE Trans. Antennas Propag.*, vol. 60, no. 11, pp. 4998–5009, Nov. 2012.

[4] G. Minatti et al., "Modulated metasurface antennas for space: Synthesis, analysis and realizations," *IEEE Trans. Antennas Propag.*, vol. 63, no. 4, pp. 1288–1300, Apr. 2015.

[5] M. Teniou, H. Roussel, N. Capet, G.-P. Piau, and M. Casaletti, "Implementation of radiating aperture field distribution using tensorial metasurfaces," *IEEE Trans. Antennas Propag.*, vol. 65, no. 11, pp. 5895–5907, Nov. 2017.

[6] M. Faenzi et al., "Metasurface antennas: New models, applications and realizations," *Sci. Rep.*, vol. 9, no. 1, pp. 1–14, Jul. 2019.

[7] M. Bodehou, K. A. Khalifeh, S. N. Jha, and C. Craeye, "Direct numerical inversion methods for the design of surface wave-based metasurface antennas: Fundamentals, realizations, and perspectives," *IEEE Antennas Propag. Mag.*, vol. 64, no. 4, pp. 24–36, Aug. 2022.

[8] A. Hessel, "General characteristics of traveling wave antennas," in *Antenna Theory*, R. E. Collin and F. J. Zucker, Eds. New York, NY, USA: McGraw-Hill, 1969, ch. 19, pp. 151–258.

[9] P. Baccarelli, S. Paulotto, D. R. Jackson, and A. A. Oliner, "A new Brillouin dispersion diagram for 1-D periodic printed structures," *IEEE Trans. Microw. Theory Techn.*, vol. 55, no. 7, pp. 1484–1495, Jul. 2007.

[10] J. R. James and P. Hall, "Microstrip antennas and arrays. Part 2: New array-design technique," *IEE J. Microw. Opt. Antennas*, vol. 1, pp. 175–181, Sep. 1977.

[11] K. Solbach and B. Adelseck, "Dielectric image line leaky wave antenna for broadside radiation," *Electron. Lett.*, vol. 19, no. 16, pp. 640–641, Aug. 1983.

[12] S. Paulotto, P. Baccarelli, F. Frezza, and D. R. Jackson, "A novel technique for open-stopband suppression in 1-D periodic printed leaky-wave antennas," *IEEE Trans. Antennas Propag.*, vol. 57, no. 7, pp. 1894–1906, Jul. 2009.

[13] J. T. Williams, P. Baccarelli, S. Paulotto, and D. R. Jackson, "1-D combline leaky-wave antenna with the open-stopband suppressed: Design considerations and comparisons with measurements," *IEEE Trans. Antennas Propag.*, vol. 61, no. 9, pp. 4484–4492, Sep. 2013.

[14] P. Burghignoli, G. Lovat, and D. R. Jackson, "Analysis and optimization of leaky-wave radiation at broadside from a class of 1-D periodic structures," *IEEE Trans. Antennas Propag.*, vol. 54, no. 9, pp. 2593–2604, Sep. 2006.

[15] S. Otto, A. Al-Bassam, A. Rennings, K. Solbach, and C. Caloz, "Radiation efficiency of longitudinally symmetric and asymmetric periodic leaky-wave antennas," *IEEE Antennas Wireless Propag. Lett.*, vol. 11, pp. 612–615, 2012.

[16] S. Otto, Z. Chen, A. Al-Bassam, A. Rennings, K. Solbach, and C. Caloz, "Circular polarization of periodic leaky-wave antennas with axial asymmetry: Theoretical proof and experimental demonstration," *IEEE Trans. Antennas Propag.*, vol. 62, no. 4, pp. 1817–1829, Apr. 2014.

[17] S. Otto, A. Al-Bassam, A. Rennings, K. Solbach, and C. Caloz, "Transversal asymmetry in periodic leaky-wave antennas for bloch impedance and radiation efficiency equalization through broadside," *IEEE Trans. Antennas Propag.*, vol. 62, no. 10, pp. 5037–5054, Oct. 2014.

[18] A. Al-Bassam, S. Otto, D. Heberling, and C. Caloz, "Broadside dual-channel orthogonal-polarization radiation using a double-asymmetric periodic leaky-wave antenna," *IEEE Trans. Antennas Propag.*, vol. 65, no. 6, pp. 2855–2864, Jun. 2017.

[19] L. Liu, C. Caloz, and T. Itoh, "Dominant mode leaky-wave antenna with backfire-to-endfire scanning capability," *Electron. Lett.*, vol. 38, no. 23, pp. 1414–1416, Nov. 2002.

[20] C. Caloz and T. Itoh, *Electromagnetic Metamaterials: Transmission Line Theory and Microwave Applications*. Hoboken, NJ, USA: Wiley, 2005.

[21] J. Liu, W. Zhou, and Y. Long, "A simple technique for open-stopband suppression in periodic leaky-wave antennas using two nonidentical elements per unit cell," *IEEE Trans. Antennas Propag.*, vol. 66, no. 6, pp. 2741–2751, Jun. 2018.

[22] P. Baccarelli, P. Burghignoli, D. Comite, W. Fuscaldo, and A. Galli, "Open-stopband suppression via double asymmetric discontinuities in 1-D periodic 2-D leaky-wave structures," *IEEE Antennas Wireless Propag. Lett.*, vol. 18, no. 10, pp. 2066–2070, Oct. 2019.

[23] A. Mallahzadeh and S. Mohammad-Ali-Nezhad, "Periodic collinear-slotted leaky wave antenna with open stopband elimination," *IEEE Trans. Antennas Propag.*, vol. 63, no. 12, pp. 5512–5521, Dec. 2015.

[24] A. Kianinejad, Z. N. Chen, and C.-W. Qiu, "A single-layered spoof-plasmon-mode leaky wave antenna with consistent gain," *IEEE Trans. Antennas Propag.*, vol. 65, no. 2, pp. 681–687, Feb. 2017.

[25] X.-L. Tang et al., "Continuous beam steering through broadside using asymmetrically modulated Goubau line leaky-wave antennas," *Sci. Rep.*, vol. 7, no. 1, pp. 1–8, Sep. 2017.

[26] M. Faenzi et al., "Realization and measurement of broadside beam modulated metasurface antennas," *IEEE Antennas Wireless Propag. Lett.*, vol. 15, pp. 610–613, 2016.

[27] F. Giusti, S. Maci, and E. Martini, "Complete open-stopband suppression for anisotropic modulated metasurfaces scanning through broadside," in *Proc. 16th Int. Congr. Artif. Mater. Novel Wave Phenomena (Metamaterials)*, Sep. 2022, pp. 166–168.

[28] F. Giusti, S. Maci, and E. Martini, "Complete open-stopband suppression in 1-D periodic metasurface leaky wave antennas," in *Proc. 16th Eur. Conf. Antennas Propag. (EuCAP)*, 2023, pp. 1–5.

[29] M. Mencagli, E. Martini, and S. Maci, "Surface wave dispersion for anisotropic metasurfaces constituted by elliptical patches," *IEEE Trans. Antennas Propag.*, vol. 63, no. 7, pp. 2992–3003, Jul. 2015.

[30] A. Oliner and A. Hessel, "Guided waves on sinusoidally-modulated reactance surfaces," *IRE Trans. Antennas Propag.*, vol. 7, no. 5, pp. 201–208, Dec. 1959.

[31] G. Minatti, F. Caminita, E. Martini, and S. Maci, "Flat optics for leaky-waves on modulated metasurfaces: Adiabatic floquet-wave analysis," *IEEE Trans. Antennas Propag.*, vol. 64, no. 9, pp. 3896–3906, Sep. 2016.

[32] M. Casaletti, "Guided waves on scalar and tensorial reactance surfaces modulated by periodic functions: A circuital approach," *IEEE Access*, vol. 7, pp. 68823–68836, 2019.

[33] D. González-Ovejero, N. Chahat, R. Sauleau, G. Chattopadhyay, S. Maci, and M. Ettorre, "Additive manufactured metal-only modulated metasurface antennas," *IEEE Trans. Antennas Propag.*, vol. 66, no. 11, pp. 6106–6114, Nov. 2018.

[34] E. Martini, F. Caminita, and S. Maci, "Double-scale homogenized impedance models for periodically modulated metasurfaces," *EPJ Appl. Metamater.*, vol. 7, p. 12, Jan. 2020.

Federico Giusti (Graduate Student Member, IEEE) was born in Poggibonsi, Italy, in 1997. He received the Laurea degree (cum laude) in electronics and communications engineering from the University of Siena, Siena, Italy, in 2021, where he is currently pursuing the Ph.D. degree.

His research interests include metasurfaces, leaky-wave antennas, electromagnetic scattering, and higher symmetric periodic structures.

Mr. Giusti was a recipient of the first prize for the Mario Sannino Award in XXIV RiNEm 2022. He has been nominated for the best paper in electromagnetics in EuCap 2023.

Stefano Maci (Fellow, IEEE) received the Laurea degree (cum laude) from the University of Florence, Florence, Italy, in 1987.

He was a co-founder of six spin-off companies. Since 1997, he has been a Professor with the University of Siena, Siena, Italy. In 2004, he was the Founder of the European School of Antennas (ESoA), a postgraduate school that presently comprises 34 courses on antennas, propagation, electromagnetic theory, and computational electromagnetics, and 150 teachers coming from 15 countries. Since 2004, he has been the Director of ESoA. From 2008 to 2015, he was the Director of the Ph.D. program in information engineering and mathematics with the University of Siena. His research activity is documented in 200 papers published in international journals (among which 100 on IEEE journals), 14 book chapters, and about 600 papers in proceedings of international conferences. His research interests include high-frequency and beam representation methods, computational electromagnetics, large phased arrays, planar antennas, reflector antennas and feeds, metamaterials, and metasurfaces.

Prof. Maci was a member of the AdCom of IEEE Antennas and Propagation Society (AP-S), the Board of Directors of the European Association on Antennas and Propagation (EurAAP), and the Antennas and Propagation Executive Board of the Institution of Engineering and Technology (IET), U.K. From 2013 to 2015, he was a member of the first National Italian Committee for Qualification to Professor. Since 2000, he has been a member of the Technical Advisory Board of 16 international conferences and the Review Board of six international journals. He was a recipient of the EurAAP Award in 2014, the IEEE Schelkunoff Transaction Prize in 2016, the Chen-To Tai Distinguished Educator Award in 2016, and the URSI Dellinger Gold Medal in 2020. He was the Chair of the Award Committee of IEEE AP-S. He has been the Technical Program Committee (TPC) Chair of the META-MATERIAL 2020 Conference and the General Chairperson of the European Conference on Antennas and Propagation (EuCAP) 2023. From 2004 to 2007, he was a Work Package (WP) Leader of the Antenna Center of Excellence (ACE; FP6-EU), and from 2007 to 2010, he was an International Coordinator of the 24-Institution Consortium of a Marie Curie Action (FP6). He founded and was the Director of the consortium FORESEEN, involving 48 European (EU) institutions. He was a Principal Investigator of the Future Emerging Technology Project "Nanoarchitectronics" of the 8th EU Framework Program. He is a Principal Investigator of the EU Program "Metamask." Since 2010, he has been a principal investigator of six cooperative projects and a university coordinator of about other 20 cooperative projects financed by European Space Agency. He has been a Distinguished Lecturer of the IEEE AP-S. He has been an EuRAAP Distinguished Lecturer of the Ambassador Program. In the last ten years, he has been invited 25 times as a key-note speaker in international conferences. He is the President of the IEEE Antennas and Propagation Society 2023. He was an Associate Editor of the IEEE TRANSACTIONS ON ANTENNAS AND PROPAGATION.

Enrica Martini (Senior Member, IEEE) received the Laurea degree (cum laude) in telecommunication engineering from the University of Florence, Florence, Italy, in 1998, and the Ph.D. degree in informatics and telecommunications from the University of Florence, and the Ph.D. degree in electronics from the University of Nice-Sophia Antipolis, Nice, France, under joint supervision, in 2002.

From 1998 to 1999, she was with the University of Florence, under a one-year research grant from Alenia Aerospazio Company, Rome, Italy. In 2002, she was appointed as a Research Associate with the University of Siena, Siena, Italy. She joined the Electromagnetic Systems Section, Ørsted DTU Department, Kongens Lyngby, Denmark, until 2007. From 2007 to 2017, she was a Post-Doctoral Fellow with the University of Siena. In 2012, she cofounded the startup Wave Up Srl, Siena, of which she was the CEO from 2016 to 2018. From 2019 to 2021, she was an Assistant Professor with the University of Siena, where she is currently an Associate Professor with the Department of Information Engineering and Mathematics. Her current research interests include metasurfaces (MTSs) and metamaterial characterization, MTS-based antennas and microwave devices, electromagnetic scattering, antenna measurements, and tropospheric propagation.

Dr. Martini was a co-recipient of the 2016 Schelkunoff Transactions Prize Paper Award, the Best Paper Award in Antenna Design and Applications at the 11th European Conference on Antennas and Propagation (EuCAP) in 2017, the Best Poster Award at the Metamaterials Congress in 2019, and the Best Paper Award in Electromagnetics at the 15th European Conference on Antennas and Propagation in 2021. In 2005, she received the Hans Christian Ørsted Post-Doctoral Fellowship from the Technical University of Denmark, Kongens Lyngby.